

The deformable multilaminate for predicting the Elasto-Plastic behavior of rocks

Hadi Haeri^{*1} and V. Sarfarazi²

¹Department of Mining Engineering, Bafgh Branch, Islamic Azad University, Bafgh, Iran

²Department of Mining Engineering, Hamedan University of Technology, Hamedan, Iran

(Received December 17, 2015, Revised March 29, 2016, Accepted April 1, 2016)

Abstract. In this paper, a multilaminate based model have been developed and presented to predict the strain hardening behavior of rock. In this multilaminate model, the stress–strain behavior of a material is obtained by integrating the mechanical response of an infinite number of predefined oriented planes passing through a material point. Essential features such as the variable deformations hypothesis and multilaminate model are discussed. The methodology to be discussed here is modeling of strains on the 13 laminates passing through a point in each loading step. Upon the presented methodology, more attention has been given to hardening in non-linear behaviour of rock in going from the peak to residual strengths. The predictions of the derived stress–strain model are compared to experimental results for marble, sandstone and dense Cambria sand. The comparisons demonstrate the ability of this model to reproduce accurately the mechanical behavior of rocks.

Keywords: multilaminate model; variable deformations hypothesis; elasto-plastic behavior

1. Introduction

It is known that the mechanical behavior of rocks generally is elasto-plastic, dilatants and strain hardening or strain softening. The identification of the post-peak behavior of rocks, in which the strain hardening occurs, under various confinement pressure is time-consuming and need to utilizing a special set up. Hence, the various elasto-plastic constitutive models based on the associated or non-associated flow rules developed for this purpose (Drucker 1959; Mroz 1963, 1966; Mandel 1964, Maier and Hueckel 1979; Chang and Hicher 2005, Antunes and Rodrigues 2008; Gao *et al.* 2010; Caputo *et al.* 2013; Samui 2013; Haeri *et al.* 2013; Schädlich and Schweiger 2013; Nemcik *et al.* 2014; Wang and Huang 2014; Haeri *et al.* 2014a, 2014b, 2014c; Haeri 2015a, 2015b, 2015c, 2015d, 2015e; Fathi *et al.* 2016; Haeri and Sarfarazi 2016a, Haeri and Marji 2016b). In previous works prediction of mechanical behavior of rocks is intricate and need to various parameters. The benefit of this paper is to introduce a simple and practical model, based on the young modulus and Poisson ratio, in multilaminate framework for derivation of non-linear behavior of rocks and dens sand. The model

*Corresponding author, Assistant Professor, E-mail: haerihadi@gmail.com

performance is then evaluated by comparing the predicted and experimental results for marble, sandstone and dense Cambria sand.

2. Strain distribution around a point

In general continuum mechanics, to define strain distribution at a point, the components are simply considered on the outer surface of a typical dx , dy , dz element. This method makes the solution to be considered uniform and the homogeneous strain distribution of the nine components over the outer surface of such dx , dy , dz element on three perpendicular coordinate axes. There is a further consideration in addition to the requirement that the displacements of a granular medium provide due to slippage/widening/closing between particles that make a contribution to the strain in addition to that from the compression of particles. Consider two neighboring points on either side of the point of contact of two particles. These two points do not in general remain close to each other but describe complex trajectories. Fictitious average points belonging to the fictitious continuous medium can be defined which remain adjacent so as to define a strain tensor. The problem presents itself differently for disordered particles compared with the ordered sphere of equal sizes. In this case, small zones may even appear in which there is no relative movement of particles. This can lead to specific behavior such as periodic instabilities known as slip-stick, creating non-homogeneity in strains and displacements. The effects of non-homogeneity in the mechanical behavior of non-linear materials are very important and must somehow be considered. Furthermore, these non-homogeneities are mostly neglected in mechanical testing because strains and stresses are usually measured at the boundary of the samples and therefore have to be considered reasonably within the whole volume. Solving non-linear problems, the mechanical behavior depends strongly on the stress/strain path as well as their histories. Upon these conditions, it may be claimed that the consideration of strain components along three perpendicular coordinate axes may not reflect the real historical changes during the loading procedure. In the most extreme case, the definition of a sphere shape element dr (instead of dx , dy , dz cube) carrying distributed strain similarly on its surface can reflect strain components on infinite orientation at a point when dr tends to zero.

The finite strain at any point in three dimensions by coordinates (x, y, z) relate to the displacements of the sides of an initial rectangular-coordinate box with sides of length dx , dy , and dz to form the three sides of a parallelepiped. This configuration of strain is established by considering the displacements of the corner points $(x, 0, 0)$, $(0, y, 0)$, and $(0, 0, z)$. This kind of strain approach leads to defining a (3×3) strain tensor including six components to present the displacement gradient matrix at a node. Accordingly, any displacement and corresponding gradient have to be defined as independent components on three perpendicular coordinate axes.

Fig. 1 shows sphere elements and a typical deformed shape. Obviously there is a certain history of displacement on any random orientation through the element. These are abbreviated in three, when a box - shape element is employed. To avoid not missing any directional information of strain, a spherical element carrying strain components over its surface as tangent and normal to the surface must be employed. This form of strain, which certainly represents a better distribution, includes all directional information. Certainly, to obtain the strain components as presented on

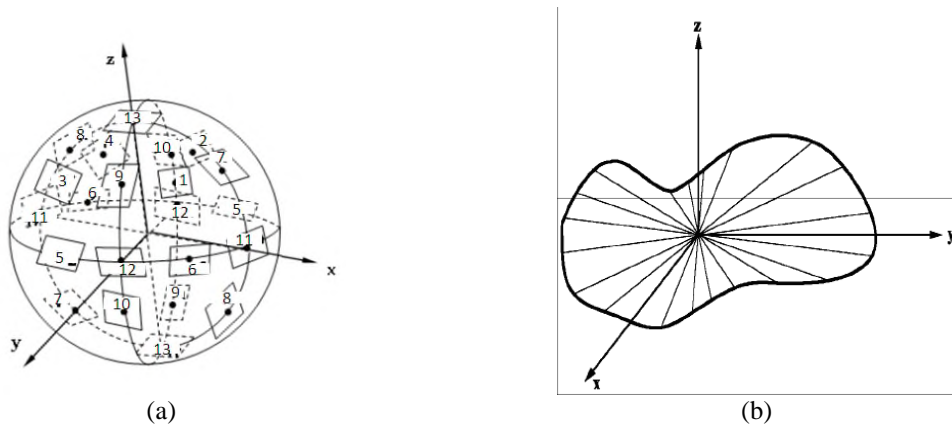


Fig. 1 (a) Sphere elements, (b) Typical deformed element

planes around box element, strain variation is integrated over the sphere surface. However, a predefined numerical integration may be employed to ease the solution.

Numerical integration generally simulates the smooth curved sphere surface to a composition of flat tangential planes, making an approximated polygon to sphere surface. The higher the number of sampling planes, the closer is the approximated surface to the sphere. Clearly, if the number of sampling planes is taken as six, the approximated surface is the same as the normal dx , dy , dz box element.

3. Multi-plane model for granular material

3.1 Background

The basic concept that a number of slip planes contribute to plastic flow was first proposed by Batdorf and Budiansky (1949) in the context of polycrystalline materials and was extended to clays by Calladine (1971). Conceptually, the idea was already discussed by Taylor (1958). A constitutive model for jointed rock masses having a finite set of parallel planes of weakness was first proposed by Zienkiewicz and Pande (1977). Assuming that soils have an infinite number of randomly oriented sets of planes, the rock model was extended by Pande and Sharma (1983) for clays and by Sadrnejad and Pande (1989) for sands. MMS was developed and implemented in the commercially available finite element code Plaxis (Brinkgreve *et al.* 2006) by Wiltafsky (2003) as a user-defined soil model. It was extended by Scharinger and Schweiger (2005) and Scharinger (2007) to include small strain stiffness effects.

3.2 Multi-plane framework

Grains in a granular materials consisting of contacts and surrounding voids are particulate media that are mostly considered continuum for ease. The accurate behavior of such particulate materials is to be investigated through macro-mechanics. However, the macro-mechanical behavior of granular materials is therefore inherently discontinuous and heterogeneous. The macroscopic as an

overall or averaged behavior of granular materials is determined not only by how discrete grains are arranged through the medium, but also by what kinds of interactions are operating among them. To investigate the macro-mechanical behavior of granular materials, certainly the spatial distribution of contact points and orientation of grains must be identified. From an engineering point of view, the main goal is to formulate the macro-behavior of granular materials in terms of macro-quantities. However, two well-known theories exist which explain the relation between macro-fields and macro-fields as macro-macro relations in a consistent manner as the average field theory and the homogenization theory. For a granular material such as sand that supports the overall applied loads through contact friction, the overall mechanical response ideally may be described on the basis of the macro-mechanical behavior of grains interconnections. Naturally this requires the description of overall stress, the characterization of fabric, representation of kinematics, development of local rate constitutive relations and evaluation of the overall differential constitutive relations in terms of the local quantities. The representation of the overall stress tensor in terms of macro level stresses and the condition, number and magnitude of contact forces has long been the aim of numerous researchers (Christofferson 1981; Nemat-Nasser 1983; Brewer 1964; Huang *et al.* 2010; Wu and Xu 2011; Ghadrhan *et al.* 2015). Multi-plane framework, by defining the small continuum structural units as an assemblage of particles and voids that fill infinite spaces between the sampling planes, has appropriately justified the contribution of interconnection forces in overall macro-mechanics. Upon these assumptions, plastic deformations are likely to occur due to sliding, separation/closing of the boundaries and elastic deformations which are the overall responses of structural unit bodies. Therefore, the overall deformation of any small part of the medium is composed of the total elastic response and an appropriate summation of sliding, and the separation/closing phenomenon under the current effective normal and shear stresses on sampling planes. These assumptions adopt overall sliding, separation/closing of inter-granular points of grains included in one structural unit are summed up and contributed as a result of sliding and separation/closing surrounding boundary planes. This simply implies yielding/failure and bifurcation response is possible over any of the randomly oriented sampling planes. Consequently, plasticity control such as yielding should be checked at each of the planes and those of the planes that are sliding will contribute to plastic deformation. Therefore, the granular material mass has an infinite number of yield functions usually one for each of the planes in the physical space. Fig. 2 shows the arrangement of artificial polyhedron simulated by real rock grains. The created polyhedrons have roughly 13 sliding planes, passing through each point in the medium. The location of tip heads of normal to the planes defining corresponding direction cosines are shown on the surface of the unit radius sphere.

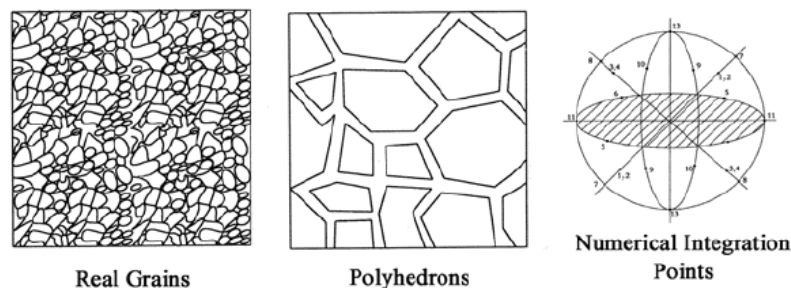


Fig. 2 Soil grains, artificial polyhedrons, and sampling points

(Planes),Weights	Direction cosines of integration points								
	l_i^1	m_i^1	n_i^1	l_i^2	m_i^2	n_i^2	l_i^3	m_i^3	n_i^3
(1),27/840	$\sqrt{1/3}$	$\sqrt{1/3}$	$\sqrt{1/3}$	$\sqrt{1/6}$	$\sqrt{1/6}$	$-\sqrt{2/3}$	$-\sqrt{1/2}$	$\sqrt{1/2}$	0.0
(2),27/840	$\sqrt{1/3}$	$-\sqrt{1/3}$	$\sqrt{1/3}$	$\sqrt{1/6}$	$-\sqrt{1/6}$	$-\sqrt{2/3}$	$\sqrt{1/2}$	$\sqrt{1/2}$	0.0
(3),27/840	$-\sqrt{1/3}$	$\sqrt{1/3}$	$\sqrt{1/3}$	$-\sqrt{1/6}$	$\sqrt{1/6}$	$-\sqrt{2/3}$	$\sqrt{1/2}$	$\sqrt{1/2}$	0.0
(4),27/840	$\sqrt{1/3}$	$\sqrt{1/3}$	$-\sqrt{1/3}$	$\sqrt{1/6}$	$\sqrt{1/6}$	$\sqrt{2/3}$	$\sqrt{1/2}$	$-\sqrt{1/2}$	0.0
(5),32/840	$\sqrt{1/2}$	$\sqrt{1/2}$	0.0	$-\sqrt{1/2}$	$\sqrt{1/2}$	0.0	0.0	0.0	1
(6),32/840	$-\sqrt{1/2}$	$\sqrt{1/2}$	0.0	$\sqrt{1/2}$	$\sqrt{1/2}$	0.0	0.0	0.0	1
(7),32/840	$\sqrt{1/2}$	0.0	$\sqrt{1/2}$	$-\sqrt{1/2}$	0.0	$\sqrt{1/2}$	0.0	1	0.0
(8),32/840	$-\sqrt{1/2}$	0.0	$\sqrt{1/2}$	$\sqrt{1/2}$	0.0	$\sqrt{1/2}$	0.0	1	0.0
(9),32/840	0.0	$-\sqrt{1/2}$	$\sqrt{1/2}$	0.0	$\sqrt{1/2}$	$\sqrt{1/2}$	1	0.0	0.0
(10),32/840	0.0	$\sqrt{1/2}$	$\sqrt{1/2}$	0.0	$-\sqrt{1/2}$	$\sqrt{1/2}$	1	0.0	0.0
(11),40/840	1	0.0	0.0	0.0	0.0	1	0.0	1	0.0
(12),40/840	0.0	1	0.0	1	0.0	0.0	0.0	0.0	1
(13),40/840	0.0	0.0	1	0.0	1	0.0	1	0.0	0.0

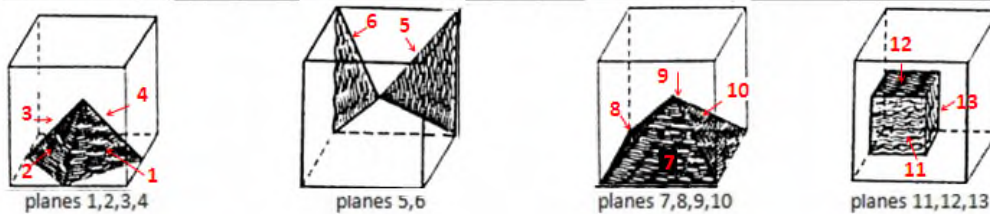


Fig. 3 Direction cosines, weighted coefficient, demonstration of 13 planes

In an ideal case, the normal integration is considered as summing up the individual macro effects corresponding to the infinite number of macro sampling planes. The choice of 13 planes for the solution of any three dimensional problems is a fair number. The orientation of the sampling planes and direction cosines of two perpendiculars on plane coordinate axes and weighted coefficients has been shown in Fig. 3.

For an employed numerical integration rule and the calculation of a stress tensor of each plane, upon the stress condition exceeds the yield limits, plastic sliding or widening/closing take place as an active plane. Therefore, one of the most important features of a multi-plane framework is that it enables the identification of the active planes as a matter of routine. The application of any stress path is accompanied by the activities of some of the 13 defined planes at any point in the medium. The values of plastic strain on all the active planes are not necessarily the same. Some of these planes initiate plastic deformations earlier than others. These priorities and certain active planes can change due to any change of direction of the stress path. A number of active planes may stop activity while some inactive ones become active and some planes may take over others with respect to the value of the plastic shear strain.

4. The variable deformations hypothesis in multilaminate framework

For application of the variable deformations hypothesis into multilaminate framework, it is assumed that the 13 sliding planes have the both of the normal and shear strains. Deformation for

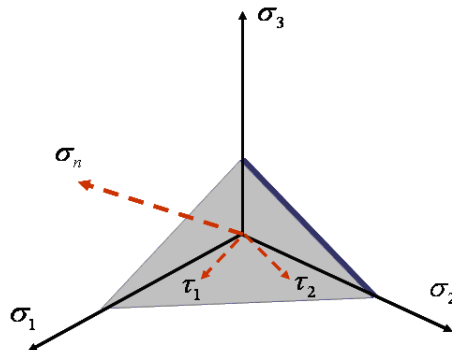


Fig. 4 The normal and shear stresses (σ_n , τ_1 and τ_2) on the one of the sampling planes

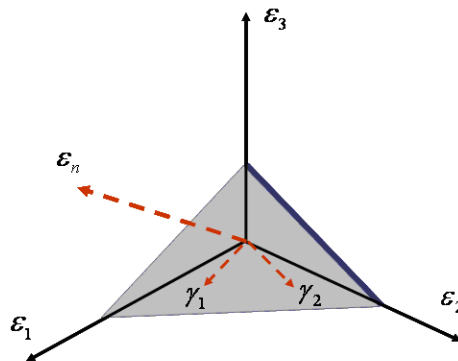


Fig. 5 The normal and shear strains (ϵ_{ni} , γ_{1i} and γ_{2i}) on the one of the sampling planes

each plane is different from other planes because the 13 sliding planes have different orientations and various direction cosines of two perpendiculars on plane coordinate axes. The summation of these deformations can be a proper representative for deformation of a point at each loading step.

4.1 Determination of the normal and shear strains in 13 sliding planes

Each sampling plane has a special direction cosine that is l_i^1 , m_i^1 , n_i^1 and two perpendicular direction cosines on plane coordinate axes that are l_i^2 , m_i^2 , n_i^2 and l_i^3 , m_i^3 , n_i^3 (Figure 3). When the specimen is subjected to tri-axial stress (σ_1 and $\sigma_2=\sigma_3$), the normal and shear stresses (σ_n , τ_1 and τ_2) is applied on the sampling planes (Fig. 4).

This normal and shear stresses can be formulated as:

$$\begin{aligned} \sigma_n^i &= \sigma_1(l_i^1)^2 + \sigma_2(m_i^1)^2 + \sigma_3(n_i^1)^2 \\ \tau_1^i &= \sigma_1 l_i^1 l_i^2 + \sigma_2 m_i^1 m_i^2 + \sigma_3 n_i^1 n_i^2 & i = 1-13 \\ \tau_2^i &= \sigma_1 l_i^1 l_i^3 + \sigma_2 m_i^1 m_i^3 + \sigma_3 n_i^1 n_i^3 \end{aligned} \tag{1}$$

The normal and shear strains (ϵ_{ni} , γ_{1i} and γ_{2i}) take place on the sampling planes As a result of these stresses (Fig. 5).

These strains are given by the following equations

$$\begin{aligned} \varepsilon_n^i &= \frac{\sigma_n^i}{E} \\ \gamma_1^i &= \frac{\tau_1^i}{G} \\ \gamma_2^i &= \frac{\tau_2^i}{G} \end{aligned} \tag{2}$$

Where E and G are Young modulus and elastic shear modulus respectively and $G=E/2(1+\nu)$; ν is the Poisson's ratio. The real strains for each sampling plane are calculated by applying of weighted coefficients (Fig. 3) into above strains as follows

$$\begin{aligned} \bar{\varepsilon}_n^i &= \frac{\sigma_n^i}{E} \times 8 \times \pi \times W_i \\ \bar{\gamma}_1^i &= \frac{\tau_1^i}{G} \times 8 \times \pi \times W_i \\ \bar{\gamma}_2^i &= \frac{\tau_2^i}{G} \times 8 \times \pi \times W_i \end{aligned} \tag{3}$$

Finally, the principal strains (ε_1 , ε_2 and ε_3) can be calculated by illustrating these local strains on the principal strain axis (Fig. 5) as follows

$$\begin{aligned} \varepsilon_1 &= \sum_{i=1}^{13} \bar{\varepsilon}_n^i l_1^i + 2 \sum_{i=1}^{13} \bar{\gamma}_1^i l_2^i + 2 \sum_{i=1}^{13} \bar{\gamma}_2^i l_3^i \\ \varepsilon_2 &= \sum_{i=1}^{13} \bar{\varepsilon}_n^i m_1^i + 2 \sum_{i=1}^{13} \bar{\gamma}_1^i m_2^i + 2 \sum_{i=1}^{13} \bar{\gamma}_2^i m_3^i \\ \varepsilon_3 &= \sum_{i=1}^{13} \bar{\varepsilon}_n^i n_1^i + 2 \sum_{i=1}^{13} \bar{\gamma}_1^i n_2^i + 2 \sum_{i=1}^{13} \bar{\gamma}_2^i n_3^i \end{aligned} \tag{4}$$

4.2 The variable deformations hypothesis

The variable deformations hypothesis is on this base that rock sample shows different behavior under constant confining pressures i.e. elastic behavior, yield behavior and plastic behavior. Fig. 6 shows the Elasto-Plastic behavior of rocks under certain confining pressure as deviator stress versus axial strain and deviator stress versus lateral strain.

Tables 1 to 3 show the parameters used in simulation.

Table 1 Parameters used in simulation

Multilaminate number (i)	Direction cosines of integration points	External loadings	Normal load on each multilaminate plane	Shear stress on each multilaminate plane in first direction	Shear stress on each multilaminate plane in second direction
1,2, ...,13	$L_i 1, m_i 1, n_i 1, l_i 2, m_i 2, n_i 2, l_i 3, m_i 3, n_i 3$	$\sigma 1$	$\sigma 2 \begin{matrix} \vdots \\ \sigma_n^i \end{matrix}$	τ_1^i	τ_2^i

Table 2 Parameters used in simulation

Normal strain in each plane	Shear strain in first direction for each plane	Shear strain in second direction for each plane	Young modulus	and elastic shear modulus	weighted coefficients for each plane
ε_n^i	γ_1^i	γ_2^i	E	G	Wi

Table 3 Parameters used in simulation

Poisson ratio	π	real strains for each plane are calculated by applying of weighted coefficients into above strains	principal strains	Volumetric strain	Deviator stress
v	3.142	$\bar{\varepsilon}_n^i, \bar{\gamma}_1^i, \bar{\gamma}_2^i$	$\varepsilon_1, \varepsilon_2, \varepsilon_3$	ΔV	$\Delta\sigma$

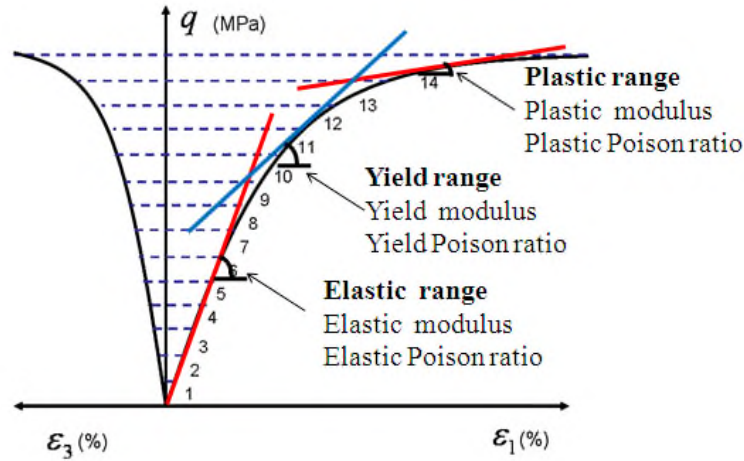


Fig. 6 The schematic curves of strain hardening behavior of rock

Three explicit ranges are identified in Fig. 6 i.e. elastic range, yield range and plastic range. Therefore, different deformation coefficients can be calculated for each range i.e. Elastic modulus, Yield modulus and Plastic modulus (Fig. 6). Also three different Poisson's ratios are defined in each range. The introduced parameters in each range are defined as follow

$$E_m = \frac{\sigma_1^{final} - \sigma_1^{initial}}{\varepsilon_1^{final} - \varepsilon_1^{initial}}, \quad \nu_m = \frac{\varepsilon_3^{final} - \varepsilon_3^{initial}}{\varepsilon_1^{final} - \varepsilon_1^{initial}} \quad (5)$$

E_m is ratio of the differential axial stress to the differential axial strain or the slope of the stress-strain curve and ν_m is the ratio of differential lateral strain to differential axial strain. m is related to three introduced range i.e. elastic range, yield range and plastic range. σ_1^{final} and $\sigma_1^{initial}$ are the final axial stress and the initial axial stress in each range, ε_3^{final} and $\varepsilon_3^{initial}$ are the final lateral strain and the initial lateral strain in each range. ε_1^{final} and $\varepsilon_1^{initial}$ are the final axial strain and the initial axial strain in each range.

To determine how deformations vary during load increasing, the stress-strain curve has been divided into n ($n=14$) equal loading steps (Fig. 6). The analysis shows that the $\epsilon_1^{n+1}-\epsilon_1^n$ increase dramatically in two stage of loading i.e. in the start of the yield range and in the start of the plastic range. This finding has been identified from stress-strain curve of different rocks (Chang and Hicher 2005). These parameters and findings are implemented into multilaminate framework to predict the elasto-plastic behavior of rocks under different confining stresses. The preference of this method is that the young modulus and poison ratio was linear in each loading steps, but its values is different from previous steps. By this approach it's possible to determine the mechanical behavior of material under external loading.

4.3 The methodology of the model calibration

To predicate the stress-strain curve of a rock sample under confining stress of σ_3 , firstly it need to extract the elastic modulus, yield modulus and plastic modulus, E_n and ν_n , from stress-strain curve of rock sample under constant confining stress of σ_3^i using Eq. (5). Then the value of new confinement stress ($\sigma_2 = \sigma_3$) is inserted into Eq. (1) and the axial stress σ_1 is applied into Eq. (1) in a small constant rate. For each increment of σ_1 , the σ_n^i , τ_1^i and τ_2^i is calculated in 13 multilaminate. At the start of the load increment, the modulus and poison ratio of elastic range are inserted into Eq. (2). From Eq.(2) and (3), the real strains for each sampling plane are calculated and the principal strains (axial and lateral strains) are determined from Eq. (4). The young modulus of plane is elastic or plastic deformation of plane, based on loading steps, in direction of normal vector. It's to be notes that $\epsilon_1^{n+1}-\epsilon_1^n$ is calculated for each increment of σ_1 . When $\epsilon_1^{n+1}-\epsilon_1^n$ increased dramatically, it shows that the yield behavior has been initiated. Therefore the modulus and poison ratio of yield range are inserted into Eq. (2) and the principal strains are calculated from Eq.(4) for each increment of σ_1 . Another increasing in $\epsilon_1^{n+1}-\epsilon_1^n$ clears that the plastic behavior has been initiated. Therefore the modulus and poison ratio of plastic range are inserted into Eq. (2) and the principal strains are calculated from Eq. (4) for each increment of σ_1 . The next dramatically increasing in $\epsilon_1^{n+1}-\epsilon_1^n$ shows that the calculations were finished. Therefore, it's possible to register the stress-strain curve of a rock sample under confining stress of σ_3 ,

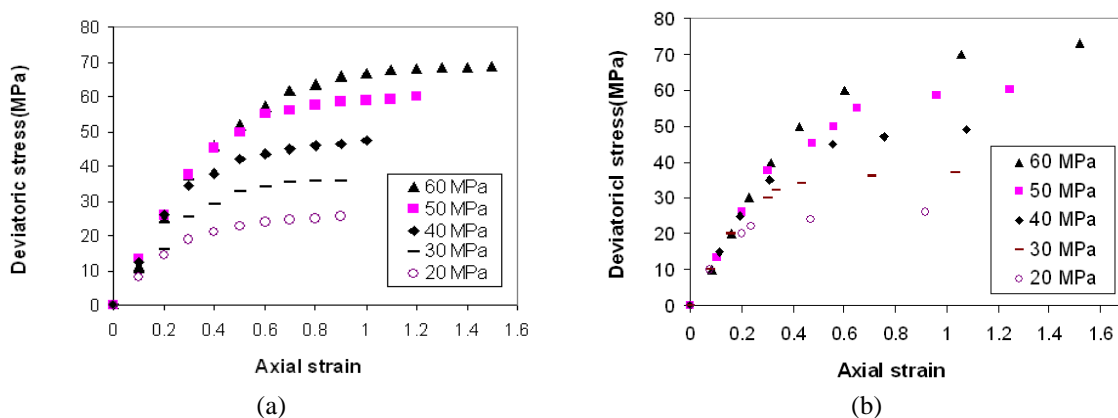


Fig. 7 Comparison of experimental with model results for marble (different confining stress);(a) test results, (b) model results

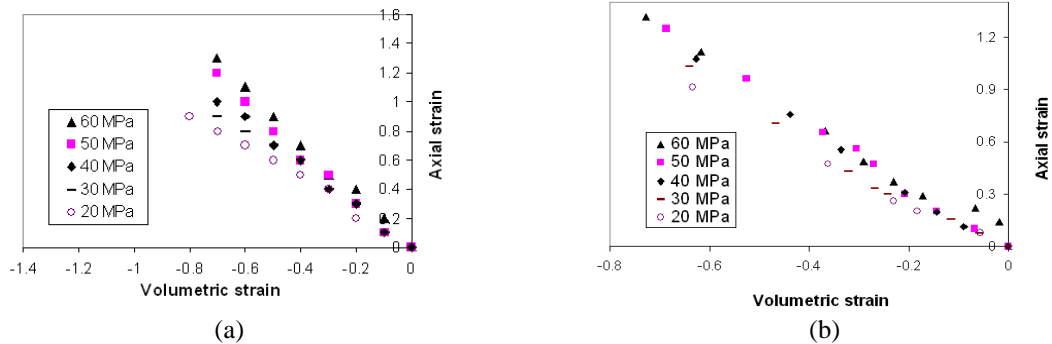


Fig. 8 Comparison of experimental with model results for marble (different confining stress);(a) test results (Chang and Hicher 2005), (b) model results

5. Verification of model results

To present the ability of the proposed model, the tri-axial test results conducted on Marble, sandstone, dense cambria sand are produced by the model.

5.1 The prediction of the elasto-plastic behavior of marble

Fig. 7(a), (b) shows the comparison of the model result with tri-axial tests for marble as stress deviator versus axial strain. Also, the comparison of volumetric strain versus axial strain are shown in Fig. 8(a), (b).

From the comparison between these Figures, the ability of the model to reproduce the main features of the marble behavior has been demonstrated.

5.2 The prediction of the Elasto-Plastic behavior of sandstone

Fig. 9(a), (b) shows the comparison of the model result with tri-axial tests for sandstone as stress deviator versus axial strain. Also, the comparison of stress deviator versus lateral strain are shown in Fig. 10(a), (b).

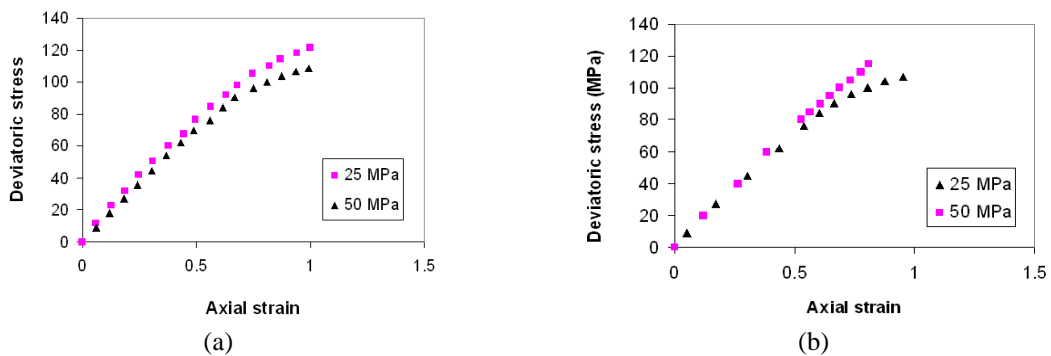


Fig. 9 Comparison of experimental with model results for sandstone (different confining stress): (a) test results (Chang and Hicher 2005); and (b) model results.

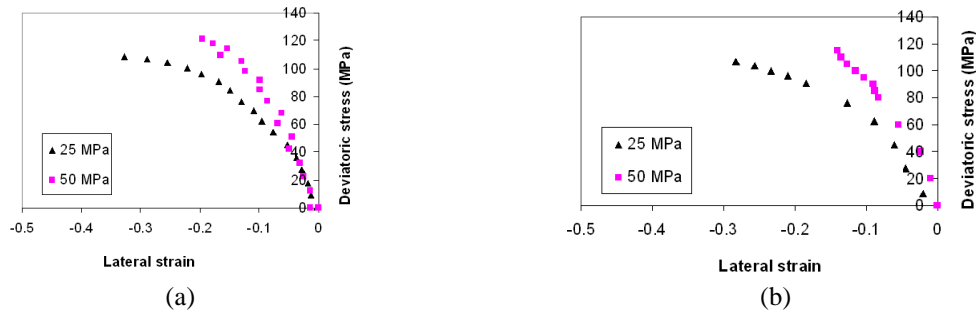


Fig. 10 Comparison of experimental with model results for sandstone (different confining stress): (a) test results; and (b) model results

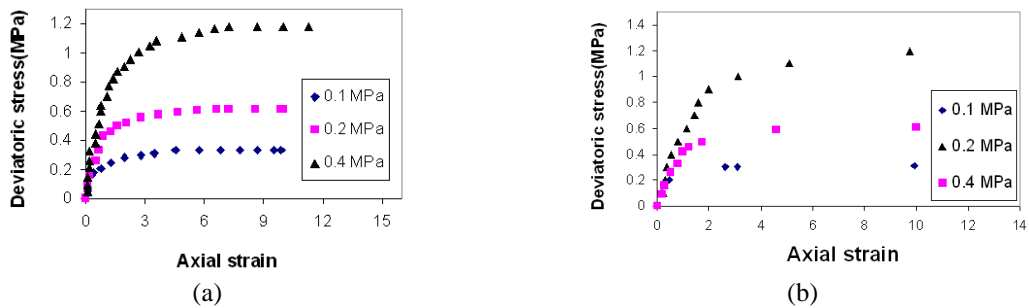


Fig. 11 Comparison of experimental with model results for dense Cambria sand (different confining stress): (a) test results ; and (b) model results

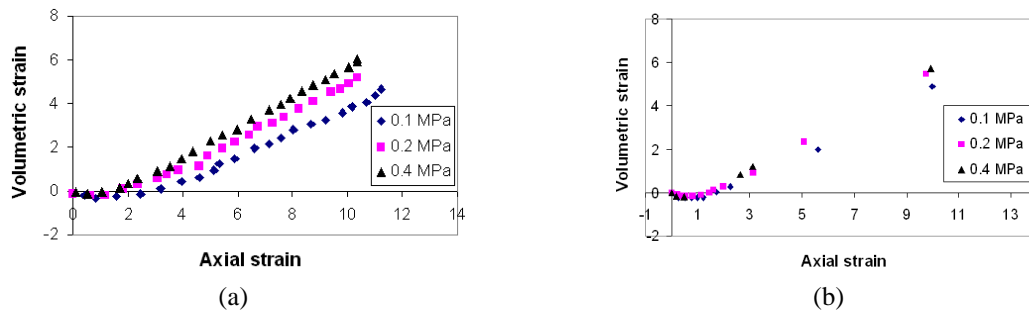


Fig. 12 Comparison of experimental with model results for dense Cambria sand (different confining stress) (a) test results; (b) model results

From the stress-strain behavior curves shown in Fig. 9 and 10, it's clear that the calculated results are very close to the test results.

5.3 The prediction of the elasto-plastic behavior of dens cambria sand

To show the capability of the proposed model in predicting the Elasto-Plastic behavior, the tri-axial test results presented by Chang *et al.* (2005) were produced and compared with the test results. Fig. 11(a), (b) shows the comparison of the model result with tri-axial tests for dens Cambria sand as stress deviator versus axial strain. Also, the comparison of volumetric strain

versus axial strain are shown in Fig. 12(a), (b). The model predicts a strain-hardening phenomenon as it assumed, also it's clear that the calculated results are very close to the test results.

Whereas the model has predicted tally results for determination of the Elasto-Plastic behavior of marble, sandstone and dense cambria sand Consequently it can be used to predict the Elasto-Plastic behavior of rocks and dense sand.

6. Conclusion

Upon the presented multilaminat framework, it needs to describe a simple relation between forces and relative displacements on any contact plane, which thus requires fewer material parameters. A multilaminat based model incorporating the variable modulus hypothesis was developed for prediction of elasto-plastic behavior of rocks. This model needs two different sets of the slope of the stress-strain curve and Poisson's ratio earned from there different stage of deformation i.e. elastic range, yield range and plastic range. The main feature of this model is that the developed model predicts the Elasto-Plastic behavior of rock without the classic plasticity formulation. Aside from modeling simplicity, the variable modulus approach is more realistic and hardening behavior can be predicted through the change of two introduced parameters. The ability of the model to reproduce the behavior of the rocks and dense sand has been demonstrated. To present the ability of the proposed model, the test results conducted on marble, sandstone and Quartz mica schist are produced by the model. A good accuracy was obtained between numerical simulations and experimental results.

References

- Antunes, F.V. and Rodrigues, D.M. (2008), "Numerical simulation of plasticity induced crack closure: Identification and discussion of parameters", *Eng. Fract. Mech.*, **75**(10), 3101-3120.
- Batdorf, S.B. and Budiansky, B. (1949), "A mathematical theory of plasticity based on the concept of slip", *National Advisory Committee for Aeronautics*, TN 1871.
- Brewer, R. (1964), *Fabric and mineral analysis of soils*. Wiley: New York, 129-158.
- Brinkgreve, R.B.J., Broere, W. and Waterman, D. (2006), *Plaxis, finite element code for soil and rock analyses*, Users Manual, PLAXIS b.v., The Netherlands.
- Calladine, C.R. (1971), "A microstructural view of the mechanical properties of saturated clay", *Geotech.*, **21**(4), 391-415.
- Caputo, F., Lamanna, G. and Soprano, A. (2013), "On the evaluation of the plastic zone size at the crack tip", *Eng. Fract. Mech.*, **103**, 162-173.
- Chang, C.S. and Hicher, P.Y. (2005), "An elasto-plastic model for granular materials with macrostructural consideration", *Int. J. Solid. Struct.*, **42**, 4258-4277.
- Christofferson, C., Mehrabadi, M.M, Nemat-Nasser, S.A. (1981), "Macromechanical description of granular behavior", *J. Appl. Mech.*, **48**, 339-344.
- Drucker, D.C. (1959), "A definition of a stable inelastic material", *J. Appl. Mech.*, **26**, 101-106.
- Fathi, A., Moradian, Z., Rivard, P. and Ballivy, G. (2016), "Shear mechanism of rock joints under pre-peak cyclic loading condition", *Int. J. Rock Mech. Min. Sci.*, **83**, 197-210.
- Ghadrdan, M., Sadrnejad, S.A. and Shaghaghi, T. (2015), "Numerical evaluation of geomaterials behavior upon multiplane damage model", *Comput. Geotech.*, **68**, 1-7.
- Haeri, H. (2015a), "Influence of the inclined edge notches on the shear-fracture behavior in edge-notched beam specimens", *Comput. Concrete* , **16**(4), 605-623,

- Haeri, H. (2015a), *Coupled experimental-numerical fracture mechanics*, Lambert academic press, Germany
- Haeri, H. (2015b), "Experimental crack analysis of rock-like CSCBD specimens using a higher order DDM", *Comput. Concrete*, **16**(6), 881-896.
- Haeri, H. (2015c), "Simulating the crack propagation mechanism of pre-cracked concrete specimens under shear loading conditions", *Strength Mater.*, **47**(4), 618-632.
- Haeri, H. (2015d), "Propagation mechanism of neighboring cracks in rock-like cylindrical specimens under uniaxial compression", *J. Min. Sci.*, **51**(3), 487-496.
- Haeri, H. and Marji, M.F. (2016b), "Simulating the crack propagation and cracks coalescence underneath TBM disc cutters", *Arab. J. Geosci.*, **9**(2), 1-10.
- Haeri, H. and Sarfarazi, V. (2016), "The effect of micro pore on the characteristics of crack tip plastic zone in concrete", *Comput. Concrete*, **17**(1), 107-127.
- Haeri, H., Marji, M.F. and Shahriar, K. (2014c), "Simulating the effect of disc erosion in TBM disc cutters by a semi-infinite DDM", *Arab J Geosci.*, **8**(6), 3915-3927
- Haeri, H., Marji, M.F., Shahriar, K. and Moarefvand, P. (2015), "On the HDD analysis of micro crack initiation, propagation, and coalescence in brittle materials", *Arab. J. Geosci.*, **8**(5), 2841-2852.
- Haeri, H., Shahriar, K., Marji, M.F. and Moaref, Vand P. (2014a), "An experimenta and numerical study of crack propagation and cracks coalescence in the pre-cracked rock-like disc specimens under compression", *Int. J. Rock Mech. Min. Sci.*, **67**, 20-28.
- Haeri, H., Shahriar, K., Marji, M.F. and Moarefvand, P. (2015), "A coupled numerical–experimental study of the breakage process of brittle substances", *Arab. J. Geosci.*, **8**(2), 809-825.
- Maier, G. and Hueckel, T. (1979), "Nonassociated and coupled flow rules of elastoplasticity for rock-like materials", *Int. J. Rock Mech., Min. Sci. Geomech. Abst.*, **16**, 77-92.
- Mandel, J. (1964), "Conditions de Stabilite et Postulat de Drucker", *Proceeding of the IUTAM Symposium on rheology and soil mechanics*, Kravichenko, J., Srieys, P.M. (Eds.), Springer-Verlag, Berlin, 58-68.
- Mroz, Z. (1963), "Non-associated flow laws in plasticity", *J. Mech.*, **2**, 21-42.
- Mroz, Z. (1966), "On forms of constitutive laws for elastic-plastic solids", *Arch. Mech. Sto.*, **18**, 1-34.
- Nakata, Y., Hyodo, M., Murata, H. and Yasufuku, N. (1998), "Flow deformation of sands subjected to principal stress rotation", *Soil. Found.*, **38**(2), 115-128.
- Nemat-Nasser, S., Mehrabadi, M.M. (1983), "Stress and fabric in granular masses, mechanics of granular materials", *New models and constitutive relations* (Eds. J.T. Jenkins and M. Satake), 1-8, Elsevier Sci. Pub.
- Nemcik, J., Mirzaghobanali, A. and Aziz, N. (2014), "An Elasto-Plastic constitutive model for rock joints under cyclic loading and constant normal stiffness conditions", *Geotech. Geol. Eng.*, **32**(2), 321-335.
- Pande, G.N. and Sharma, K.G. (1983), "Multi-laminate model of clays-a numerical evaluation of the influence of rotation of the principal stress axes", *Int. J. Numer. Anal. Method. Geomech.*, **7**(4), 397-418.
- Sadrnejad, S.A. and Pande, G.N. (1989), "A multilaminate model for sands", *Proceedings of the 3rd International Symposium on Numerical Models in Geomechanics (NUMOG)*, Niagara Falls, Canada, Pietruszczak S, Pande GN (eds). Elsevier: London, 17-27.
- Samui, P. (2013), "Multivariate Adaptive Regression Spline (Mars) for prediction of elastic modulus of jointed rock mass", *Geotech. Geol. Eng.*, **31**(1), 249-253.
- Schädlich, B. and Schweiger, H.F. (2013), "A multilaminate constitutive model accounting for anisotropic small strain stiffness", *Int. J. Numer. Anal. Method. Geomech.*, **37**(10), 1337-1362.
- Scharinger, F. (2007), "A multilaminate model for soil incorporating small strain stiffness", Ph.D. Thesis, Gruppe Geotechnik Graz, Heft 31, Graz University of Technology, Austria.
- Scharinger, F. and Schweiger, H.F. (2005), "Undrained response of a double hardening multilaminate model for soils", *Proceedings of the 11th International Conference of the International Association of Computer Methods and Advances in Geomechanics (IACMAG)*, Turin, Italy, Barla G, Barla M (eds). Patron Editore: Bologna, 505-512.
- Taylor, G.I. (1958), "Plastic strain in metals", *J. Inst. Metal.*, **62**, 307-324 (Reprinted in the Scientific Papers of G. I. Taylor 1. Cambridge University Press: Cambridge, U.K.).
- Varadarajan, A., Sharma, K.G, Hashemi, M. Strain (2003), "Softening behaviour of a schistose rock mass

- under triaxial loading”, Technology roadmap for rock mechanics, S. Africa Inst. Min. Metall.
- Wang, T.T. and Huang, T.H. (2014), “Anisotropic deformation of a circular tunnel excavated in a rock mass containing sets of ubiquitous joints: Theory analysis and numerical modeling”, *Rock Mech. Rock Eng.*, **47**(2), 643-657.
- Wiltafsky, C. (2003), “A multilaminate model for normally consolidated clay”, Ph.D. Thesis, Gruppe Geotechnik Graz, Heft 18, Graz University of Technology, Austria.
- Wu, J.Y. and Xu, S.L. (2011), “An augmented multicrack elastoplastic damage model for tensile cracking”, *Int. J. Solid. Struct.*, **48**(18), 2511-2528.
- Xin, G., Hangong, W., Xingwu, K. and Liangzhou, J. (2010), “Analytic solutions to crack tip plastic zone under various loading conditions”, *Eur. J. Mech.-A/Solid.*, **29**(4), 738-745.
- Yi, H., Jingjie, C. and Gang, L. (2010), “A new method of plastic zone size determined based on maximum crack opening displacement”, *Eng. Fract. Mech.*, **77**(14), 2912-2918.
- Zienkiewicz, O.C. and Pande, G.N. (1977), “Time-dependent multilaminate model of rocks-a numerical study of deformation and failure of rock masses”, *Int. J. Numer. Anal. Method. Geomech.*, **1**(3), 219-247.